Experimental investigation of reinforced concrete exterior beam-column subassemblages for progressive collapse

Li, Bing.; Yap, Sim Lim.

2011

Yap, S. L., & Li, B. (2011). Experimental investigation of reinforced concrete exterior beam-column subassemblages for progressive collapse. ACI Structural Journal, 108(5), 542-552.

https://hdl.handle.net/10356/95273

ACI STRUCTURAL JOURNAL TECHNICAL PAPER

Title no. 108-S51

Experimental Investigation of Reinforced Concrete Exterior Beam-Column Subassemblages for Progressive Collapse

by Sim Lim Yap and Bing Li

This paper presents experimental investigations on the performance of reinforced concrete (RC) exterior beam-column subassemblages under progressive collapse scenario (loss of exterior ground column). The amount of resistance the beam-column subassemblages could provide the structural frame against progressive collapse is of great value in predicting the performance of buildings and for determining the stability of buildings during search-and-rescue operations. Two series of test specimens were tested under monotonic loading to simulate gravity load on the damaged structure after a blast event (assuming the damaged structure remained standing). In the first series (NS series), the overall performance of the beam-column subassemblages based on as-built detailing of structures commonly found in Singapore were assessed. In the second series (LS series), improvements/modifications were made to the as-built design by incorporating some seismic detailing. The experimental results highlighting behavior, such as force-displacement responses, crack patterns, and failure mechanisms, are discussed and the overall performance of the two series were compared and evaluated. In this investigation, extensive instrumentation both internal and external allowed for detailed analysis of the response of the beam-column subassemblage, which is summarized in the paper.

Keywords: beam-column; collapse; reinforced concrete.

INTRODUCTION

Progressive collapse has been of great concern to structural engineers, especially with the wide publicity of recent cases. ASCE 7-02[1] defines progressive collapse as the spread of an initial local failure from element to element, which eventually results in the collapse of an entire structure or a disproportionately large part of it. In less technical terms, it is often thought of as the domino effect. One of the earliest recorded incidents is the collapse of Ronan Point Apartment,[2] London, UK, in 1968. This is followed by the terrorist attacks on the Murrah Building,[3] Oklahoma City, Oklahoma, in 1995 and, more recently, the World Trade Center,[4] New York City, New York, in 2001.

The Ronan Point Apartment incident brought about a new design philosophy with regard to progressive collapse. Since then, many codes and standards have attempted to provide design guidelines in response to this collapse phenomenon. Two of the more comprehensive guidelines that provide progressive collapse analysis were published by the General Services Administration (GSA) and the Department of Defense (DOD). The GSA[5] adopted a threat-independent approach, where key load-bearing elements are systematically removed and the remaining structure is designed based on the redistributed load. At the very least, the building must be able to withstand the loss of at least one of the vertical load-bearing members without causing progressive collapse. The DOD[6] employed two methods: 1) the tie force method, mechanically tying the building together, thereby enhancing continuity and ductility; and 2) the alternate path method, which adopted an approach similar to that of GSA[5] by designing the building based on redistributed load after the removal of vertical load-bearing elements. Despite the long history of studies conducted on progressive collapse, the majority of the studies were based on case studies of actual collapses and numerical and finite element analyses. There are many drawbacks in the aforementioned methods, however. For instance, the influence of variables cannot be controlled and determined through case studies, whereas numerical and finite element analyses often require calibration and validation. Only recently have researchers begun to investigate progressive collapse through controlled experiments, offering to fill the missing gap in research. Furthermore, with prior knowledge available from numerical and finite element analyses, experimental investigation on specific critical variables that influence the structure's performance can be performed economically. One such controlled experiment was conducted by Yi et al.,[7] where the progressive collapse resistant behavior of reinforced concrete (RC) frame structures was investigated.

In the study of progressive collapse, although numerous damage scenarios can be assumed, one of the most probable scenarios is the loss of exterior ground column. The loss of the supporting column changes the boundary conditions of the structure, causing it to seek alternate load paths to redistribute loads, thus maintaining equilibrium. The important question now is whether the structural elements have the capacity for load redistribution and the ability to withstand the increase in load. Otherwise, they will fail due to overloading, resulting in progressive collapse.

The beam-column joint is one of the critical elements responsible for resisting and distributing load. Extensive controlled experimental investigations have been carried out, especially in the area of seismic performance. However, there is no known literature on controlled experiments relating to the performance of beam-column joints in a post-blast scenario under progressive collapse. It is important to understand that failure in joints will greatly affect the ability of the structure to redistribute loads. Of the different type of joints, the exterior beam-column joint is especially critical due to the following reasons:

1. The loss of an exterior ground column directly affects the vertical load transfer path of the above column.

2. The exterior beam-column subassemblages are subjected to a complete change in the direction and distribution of the bending moment, which the elements were not designed for.

ACI Structural Journal, V. 108, No. 5, September-October 2011.

Sim Lim Yap *is an Engineer in the Defense Science and Technology Agency (DSTA), Singapore. He received his BEng and MEng from the Nanyang Technological University, Singapore. His research interests include reinforced concrete structures, particularly progressive collapse.*

ACI member **Bing Li** *is an Associate Professor in the School of Civil and Environmental Engineering at Nanyang Technological University. He received his PhD from the University of Canterbury, Christchurch, New Zealand. His research interests include reinforced concrete and precast concrete structures, particularly the design of earthquake- and blast-resistant structures.*

3. Failure in the subassemblages either in beam (hinging), column (hinging), or joint (shear failure) will result in the distribution of moments into the building, causing internal members to be overloaded further and possibly collapse.

Figures 1(a) and (b) illustrate the change in bending moments of a structural frame before and after the loss of the exterior ground column, respectively. Figure 1(c) shows the possible increase in the bending moment of a structure frame with the failure of the exterior beam-column subassemblages (in either of the failure modes mentioned previously).

In assessing a building's stability during search-and-rescue operations, the amount of resistance the beam-column subassemblage can provide the damaged structural frames against progressive collapse in terms of load and moment transfer is of great importance. Furthermore, it worth noting that debris, which will fall as a result of the blast, and the personnel and equipment associated with the search-and-rescue teams will add to the load of the structure. These increase the level of uncertainty in regard to the stability of the damaged structure, as the load conditions on different stories would most likely be different.

In Singapore, most buildings, other than military and diplomatic facilities, are not designed against threats such as terrorist bomb attacks. Therefore, the performance of beam-column subassemblages is especially important. Furthermore, beam-column joints are not generally designed in practice because there is no requirement in CP 65[8]—the Singapore design code—which is based on BS 8110-1:1997.[9]

RESEARCH SIGNIFICANCE

This study presents the test results of six exterior beam-column subassemblages tested under monotonic loading. The test setup was specially designed to ensure that boundary conditions were representative of the actual scenario (loss of exterior column). The amount of resistance the subassemblages could provide the damaged structure against progressive collapse and the associated failure mode will provide valuable information to the limited data on the collapse potential of RC frame structures. A comparison between the as-built design and the improved design not only provides information with regard to the amount of improvement possible through incorporating seismic detailing but also, more importantly, their limitation toward progressive collapse mitigation. Furthermore, the validation and calibration of test data will enhance the accuracy and reliability of finite element analysis.

EXPERIMENTAL PROGRAM

Establishment and design of test setup

The test setup and the overall dimensions of the test specimens were designed to ensure that loading and boundary conditions were representative of the actual scenario. These were determined through the bending moment diagram (Fig. 1(b)) and the

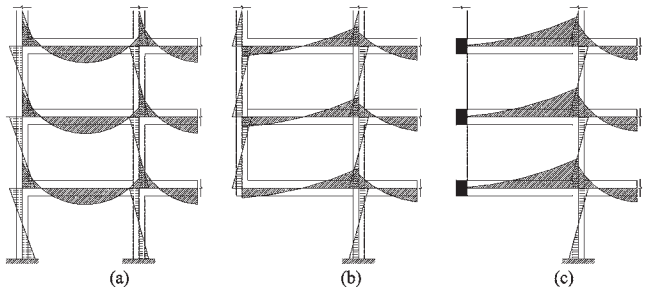

Fig. 1—Illustration of moment redistribution.

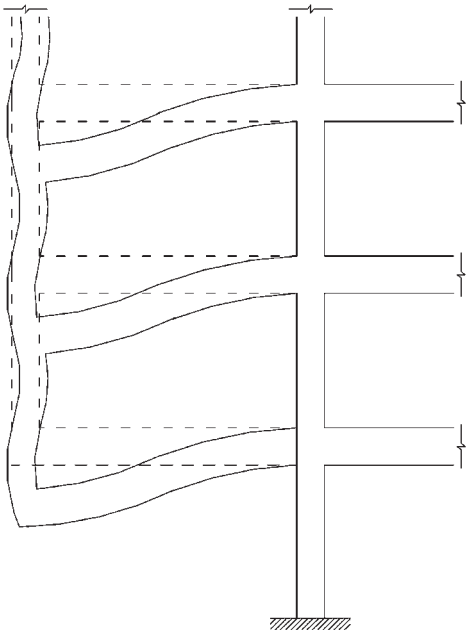

Fig. 2—Illustration of deformed shape.

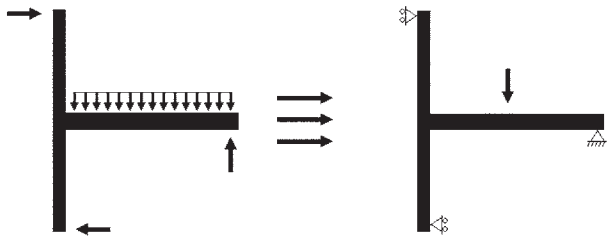

Fig. 3—Illustration of free body diagram and representative simplified boundary condition of subassemblage.

deformed shape (Fig. 2) of the assumed structural frame. The points of contraflexure were chosen to be the end boundaries of the subassemblages because of the zero moment condition that can be easily achieved in the test setup. Figure 3 shows the free body diagram and the representative simplified boundary conditions of the subassemblage.

The test frame consisted of two steel frames, a series of steel assemblies, and one hydraulic jack. The configuration of the loading frame is shown in Fig. 4. The main consideration in the design of the loading frame was to achieve the required boundary conditions of the column element (freedom of movement [downward] in the direction of the column axis).

The feasibility during the setup process, given the laboratory constraints, was also considered. In the setup, the column element was positioned horizontally and the beam element was positioned vertically. The column was supported by a pair of rollers at both ends, allowing movement (left, representing downward) along the column axis and was guided by a set of supporting steel assemblies. The pinned condition at the beam boundary was achieved with a solid steel rod through the beam section, which allowed rotation in the direction perpendicular to the column axis. The steel rod was supported at both ends by two steel frames. Gravity loading on the beam simulating the floor service load on the structure after a blast event was applied using a hydraulic jack as a point load. The steel frames and all other steel assemblies were fastened to the strong floor using bolts and pretensioned steel rods.

Test procedure and loading method

Before the commencement of any loading sequence, the test specimen was painted with a thin coat of whitewash to permit better crack observation. All instrumentation, which will be described in the following sections, were calibrated in positions and initialized. The test procedure involved loading the beam monotonically to determine the resistance of the beam-column subassemblage.

Loading on the beam was increased to 10 kN (2.25 kips) per loading step (force-controlled) through the action of the hydraulic jack to determine the overall resistance of the beam-column subassemblage. In each loading step, a complete set of readings, which will be described in the following sections, was taken with the data logger. Crack patterns on the surface of the test specimen were drawn after each loading step, and photographs were taken for detailed observation and analysis. Tests were terminated once a 20% drop in the overall strength was observed.

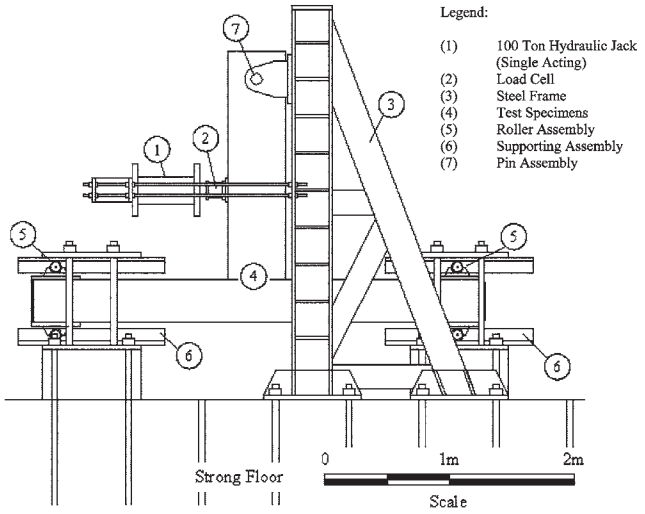

Fig. 4—Loading frame: full configuration. (Note: 1 ton = 2.25 kips; 1 m = 3.28 ft.)

Test specimens and material data

Two series of exterior beam-column subassemblages, referred to as the NS series (with as-built detailing) and the LS series (with improved detailing), were designed to study the effects on varying the amount of transverse reinforcement in each series. The additional amount of resistance the "improved design" could provide the damaged structure against progressive collapse was determined. It was noted that in the improved design (LS series), through incorporating some seismic detailing, the amount of longitudinal reinforcement in the beam was increased and transverse reinforcement was provided in the joint region. Details of the test specimens are summarized in Table 1. The reinforcement detailing was detailed in accordance with CP 65.[8]

The overall dimensions (typical for both series) and cross-sectional details of the specimens are shown in Fig. 5. In the NS series, transverse reinforcements in the beams at one beam depth length from the face of the columns were varied. Transverse reinforcements were hoop stirrups with 90-degree blast. No transverse reinforcement was provided in the joint regions. Lapping of the column longitudinal bars just above the floor level was included in this series. High-yield steels were used for the longitudinal reinforcements, whereas mild steel was used for the transverse reinforcements. Table 2 shows the mechanical tensile properties of the reinforcing steel. The concrete compressive strength was 30 MPa (4300 psi). In the LS series, transverse reinforcements (beams and columns) were varied in the joint regions. Transverse reinforcements were hoop stirrups with 135-degree bends. Column longitudinal bars were continuous throughout the floor level. High-yield steels were used for both the longitudinal and transverse reinforcements.

Instrumentation

To monitor the response of the test specimen, extensive measuring devices were installed both internally and externally. A total of 70 data channels were active during the testing process. A load cell was used to measure the applied force on the beam while displacements at the midpoint of the beam where loading was applied and at the column end were measured using linear variable differential transformers (LVDTs). A series of LVDTs and linear potentiometers were also placed at various locations of the beam-column subassemblage to measure the different types of internal deformation, such as fixed-end rotation, curvature, and

Table 1— Design parameters of tested specimens

Series	Label	Element		Longitudinal reinforcement, %				Transverse reinforcement, %		
					Beam			Column ($1h_c$ from face of beam)	Beam ($1h_b$ from face of column)	Joint, %
		Column	Beam	Column	Top	Bottom	Total			
NS	01	Height = 2175 mm Cross section = 350 x 350 mm	Length = 1800 mm Cross section = 470 x 250 mm	8T20 (2.35)	3T25 (1.39)	2T25 (0.93)	5T25 (2.32)	0.149	0.314	0
	02								0.419	
	03								0.628	
LS	01			8T20 (2.35)	3T25 (2.35)	3T25 (1.39)	6T25 (2.79)	0.383	0.314	0.383
	02							0.510	0.419	0.510
	03							0.766	0.628	0.766

Notes: Nominal column transverse reinforcement = 0.149% (refer to Fig. 5 for illustration; nominal beam transverse reinforcement = 0.314% (refer to Fig. 5 for illustration; 1 mm = 0.04 in.

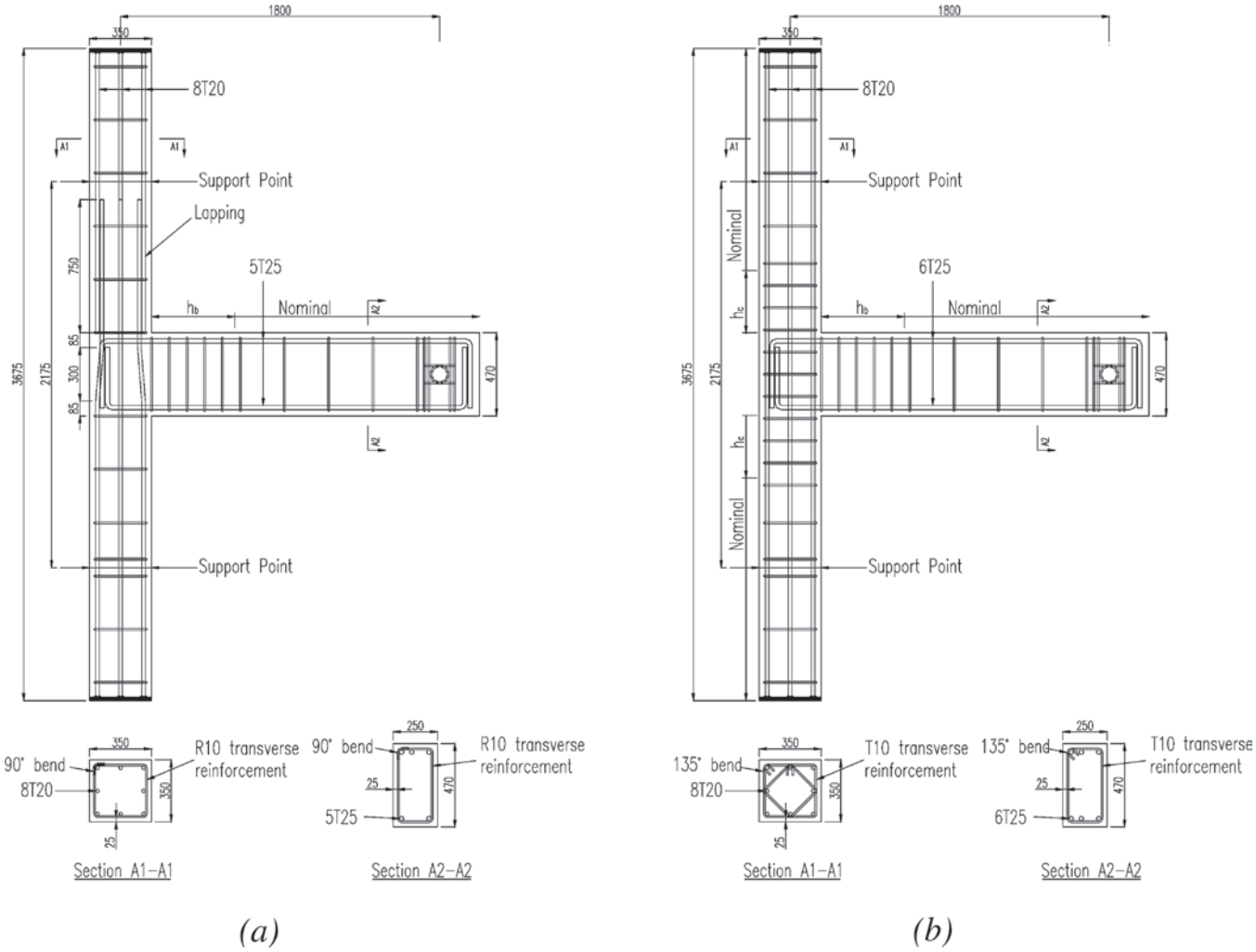

Fig. 5—Dimensions and cross-sectional details: (a) NS series; (b) LS > series. (Note: All dimensions are in mm;1 mm = 0.04 in.).

diagonal deformations. In total, 40 electrical resistance strain gauges were mounted on the reinforcement at strategic locations, in particular the joint to monitor joint shear and yield penetration.

TEST RESULTS

Global behavior

The global behavior of the test specimens was observed based on their crack patterns. In general, the crack patterns were divided into four areas: 1) joint shear crack; 2) flexural crack; 3) beam shear crack; and 4) column shear crack. The final crack patterns of the specimens are shown in Fig. 6. As it is impossible to describe in detail the crack development for all the specimens in this study, the differences in crack development between the specimens of the two series are presented instead.

Specimens from both the NS and LS series experienced severe joint cracking at the final stage of the tests. The crack patterns, however, were distinctly different in the joint panel between the specimens of the two series. For the NS series specimens, one dominant diagonal shear crack developed between the two compression zones, as illustrated in Fig. 7(b). For the LS series specimens, although there was a dominant corner-to-corner diagonal shear crack, additional diagonal shear cracks of gentler inclinations were also observed in the joint region, as illustrated in Fig. 7(a). It was suggested that the major difference in the crack patterns was due to the presence of joint transverse reinforcement. Figures 7(a) and (b) show the possible internal forces flow paths that were superimposed onto the crack patterns of Specimens LS02 and NS02, respectively.

In an exterior beam-column joint, reliance for the beam bar anchorage is placed primarily on a standard hook rather than on the straight portion of the beam bars between the inner column face and the hook. This resulted in a force introduced into the joint core concrete by means of bearing and bond within the bend.

In the NS series specimens, as illustrated in Fig. 7(b), the reinforcement detailing is arranged such that a diagonal

Table 2—Measured properties of reinforcing steel

Type	Grade, MPa	Yield strength f_y, MPa	Yield strain ε_y, 10^{-6}	Ultimate strength f_u, MPa
R10	250	385.1	2101.1	522.0
T10	460	480.0	2718.8	624.0
T20	460	512.0	2545.0	606.6
T25	460	559.0	2800.0	632.0

Notes: R10 is plain round bar of 10 mm diameter; T10 is deformed high-strength bar of 10 mm diameter; T20 is deformed high-strength bar of 20 mm diameter; T25 is deformed high-strength bar of 25 mm diameter; each value was obtained from average of three tests; 1 MPa = 145 psi; 1 mm = 0.04 in.

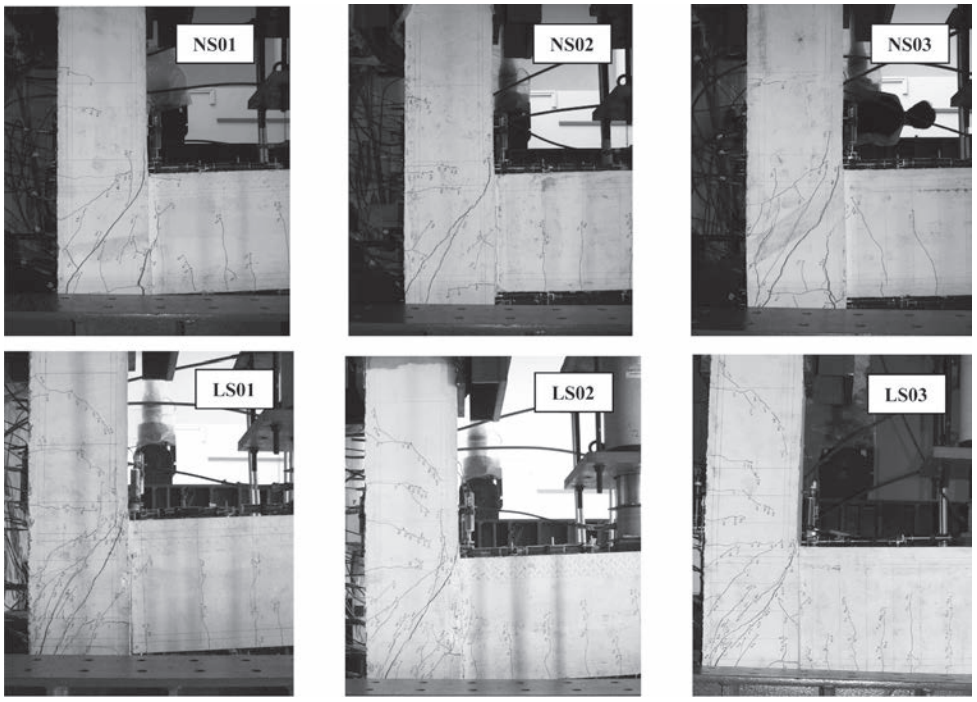

Fig. 6—Observed crack patterns of Specimens NS01, NS02, NS03, LS01, LS02, and LS03.

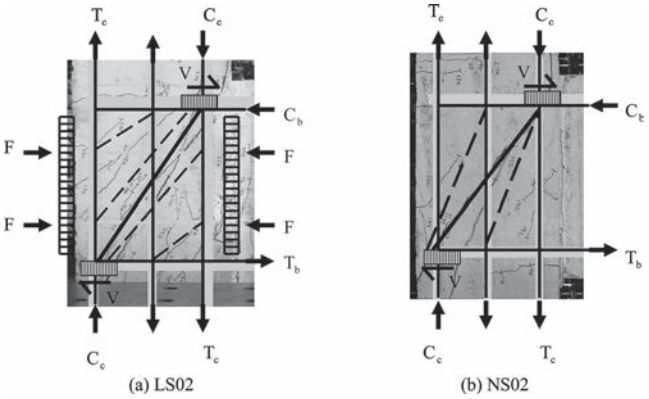

Fig. 7—Illustration of internal force flow.

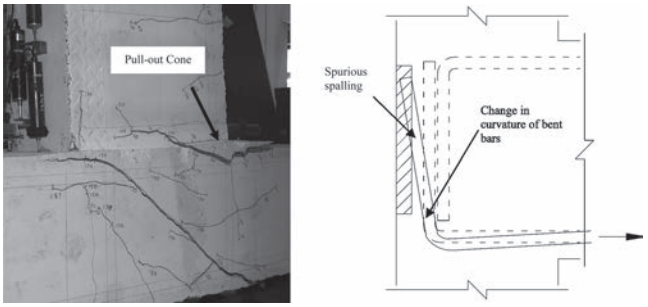

Fig. 8—Illustration of pullout failure (Specimen NS01).

compression strut, which is the main shear-resisting mechanism, can develop between the bend of the bottom beam bars and the upper right-hand corner of the joint, where compression forces in both the horizontal and vertical directions are introduced by the beam and column, respectively. Tensile stresses are generated at right angles to this compression strut, which is responsible for the diagonal tension cracking in the joint core.

For the joint reinforcement configuration of the LS series specimens, alternate stress paths may be possible, in which multiple struts with less inclination may develop within the transverse links in the joint region, as illustrated in Fig. 7(a). This is only possible when adequate joint transverse reinforcement is placed in the effective zone to provide the necessary horizontal tie forces to balance the forces from the diagonal compressive strut, developing the truss mechanism. The strain profiles observed in the joint stirrups of the LS series specimens during the test support these alternate stress paths, which accounted for the differences in the crack patterns.

Flexural cracks at the beam-column interface, which represent the fixed-end rotation of the beam, were significantly different between specimens of both series as well. For specimens of the NS series, bond splitting cracks along the bottom beam bars together with flexural cracks at the beam-column interface, which extended across the entire depth of the beam, were developed at the early stages of the test. Following that, steel stress increased rapidly, leading to differential movement (slippage) between the steel and the concrete. On further loading, slippage manifested itself, which ultimately led to bar pullout, as evidenced by the formation of the pullout cone and spurious spalling action of bent bars due to curvature changes under force, as shown in Fig. 8. These failure patterns, however, were not observed in the LS series specimens. Furthermore, bond splitting cracks along the bottom beam bars occurred at later stages. These differences were suggested to be due to the increase in the bottom longitudinal reinforcement ratio from 0.93 to 1.39%, which resulted in a higher bending moment capacity and, in turn, rotational capacity. It was also suggested that the presence of transverse reinforcements in the joint region prevented the bottom longitudinal bars from being pulled out and the change in curvature of the bent bars.

Force-deflection response

Figure 9 shows the force-deflection response of the test specimens. Deflection is defined as downward movement of the joint with reference to the contraflexure point of the beam element. The performances of the subassemblages were assessed based on strength (ultimate capacity), general profile of the curves, and overall deflection of the test specimens.

General profile—In general, force-deflection profiles belonging to specimens of the same series were similar. There were some significant differences, however, in the trends of the curves between specimens of the different series. These differences were related to the different mechanisms, which will be described in subsequent sections, and provided resistance to the increase in forces at different stages of the test. Once these mechanisms reached capacity or failed, stiffness degradation and, eventually, strength degradation occurred.

For the LS series specimens, no distinct change in the gradient was observed. Changes were observed to be gradual, showing slow and controlled stiffness degradation up to the point of yield. The observed trend suggested that the presence of the transverse reinforcement in the joint region provided additional mechanisms for resisting joint shear forces. Failure of one of the mechanisms did not result in severe stiffness or strength degradation. For NS series specimens, the only mechanisms resistance joint shear was the concrete. Therefore, once the diagonal tensile strength of concrete was reached, tensile crack will occur and propagate, resulting in an abrupt decrease in stiffness and thus the gradient of the slope.

The observed differences in the gradient of slope after attaining maximum load were suggested to be associated with the dominant failure mode of the specimens. For the NS series specimens, after attaining maximum load, severe strength degradation signified by the steep negative gradient occurred immediately. This was the failure characteristic associated with bond failure of the bottom beam reinforcing bars at the joint region. For the LS series specimens (with the exception of Specimen LS03), the gradient of the slope remained relatively gentle for an extended period of time, showing ductile behavior. This failure characteristic followed the stress-strain characteristic of the joint transverse reinforcing steels bars, which was suggested to be the last mechanism resisting joint shear failure for Specimens LS01 and LS02. The observed differences for Specimen LS03 were explained under the Joint behavior section.

Strength (ultimate capacity) and deflection—The maximum strength of Specimens NS01, NS02, NS03 obtained from the tests were 184, 188, and 191 kN (41.4, 42.3, and 43.0 kips), respectively. Between Specimens NS01 and NS02, the increase in strength was 2.2%. Between Specimens NS02 and NS03, the difference was 1.6%. Therefore, this indicates that the influence of transverse reinforcements in the beams and columns on the strength of the specimens was insignificant.

When comparing the deflection of the NS series specimens, however, it was observed that between Specimens NS01 and NS02, there was a reduction in deflection by approximately 13.7% (from 44.6 to 38.5 mm [1.78 to 1.54 in.]). Between Specimens NS02 and NS03, there was a reduction by 8.1% (from 38.5 to 35.4 mm [1.54 to 1.42 in.]). Therefore, it is suggested that by increasing the amount of transverse reinforcements in the beams and columns, deflection can be reduced through controlling the deformations of the elements.

For the LS series specimens, between Specimens LS01 and LS02 and between Specimens LS02 and LS03, there

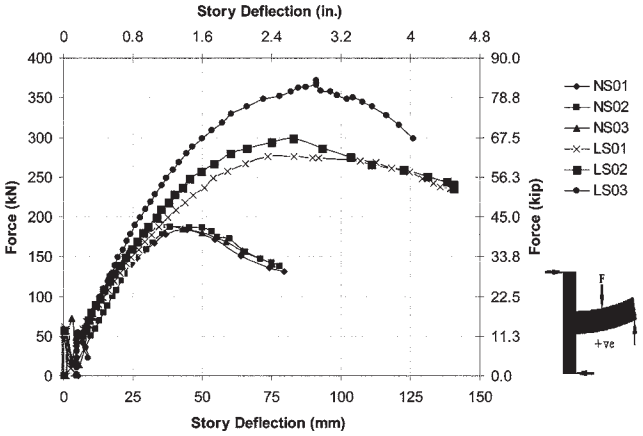

Fig. 9—Comparison of force-deflection response.

Table 3—Specimen strength at different stages

Specimen	Joint cracking, kN	Specimen failure, kN	Difference, %
NS01	130.0	184.0	29.3
NS02	128.4	188.0	31.7
NS03	134.1	191.1	29.8
LS01	149.0	276.3	46.1
LS02	149.7	298.6	50.0
LS03	149.0	371.7	59.9

Note: 1 kN = 0.225 kips.

was an increase in the overall strength of the specimens by 8.1% and 24.5%, respectively. This suggests that the amount of reinforcement in the joint region, together with the additional longitudinal beam bar, significantly influences the overall strength of the beam-column subassemblages.

The deflections of the LS series specimens were observed to have increased. An increase of 12.2% and 5.2% was observed between Specimens LS01 and LS02 and Specimens LS02 and LS03, respectively. When comparing the percentage of increase in strength and deflection, it was observed that between Specimens LS02 and LS03, an increase in strength of 24.5% only resulted in an increase in deflection of 5.2%. Therefore, the influence on transverse reinforcement in reducing the overall deflection, as discussed previously, is still considered valid for the LS series specimens, even though an increase in overall deflection was observed.

Between the two different series, the increase in overall strength by employing the improved design ranges from 50.2% (between Specimens NS01 and LS01) to 102% (between Specimens NS01 and LS03). The increase in strength was suggested to be primarily contributed by the combined effect of the additional transverse reinforcement in the joint region and the increase in beam longitudinal reinforcement.

In addition to the differences in the failure load of the specimens, another noteworthy observation was the differences in the load gap between joint cracking and failure. Table 3 shows the load of the specimens at joint cracking and at failure. The load at joint cracking for the LS series specimens was defined as the load at which diagonal shear cracking in the joint was fully developed.

It was observed that for the NS series specimens, after the occurrence of joint cracking, an additional increase in load prior to failure was relatively consistent at approximately 30%. This was because joint cracking was predominantly influenced by the tensile strength of the concrete within

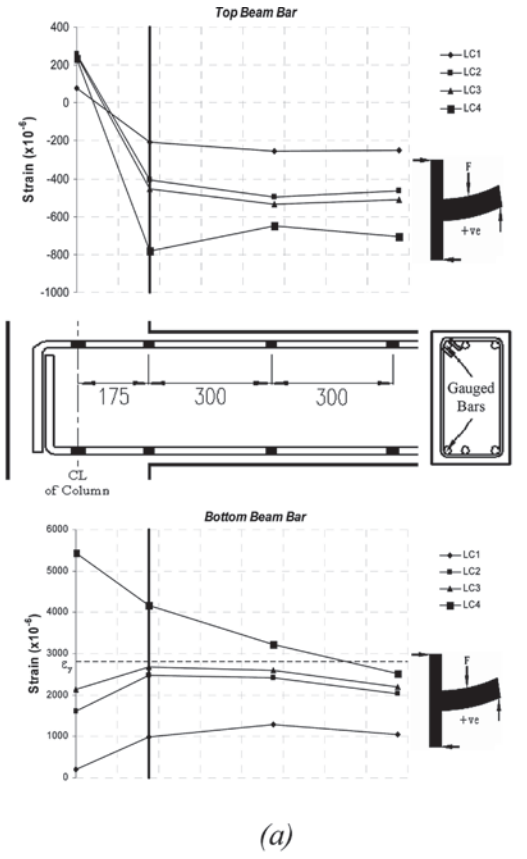

(a)

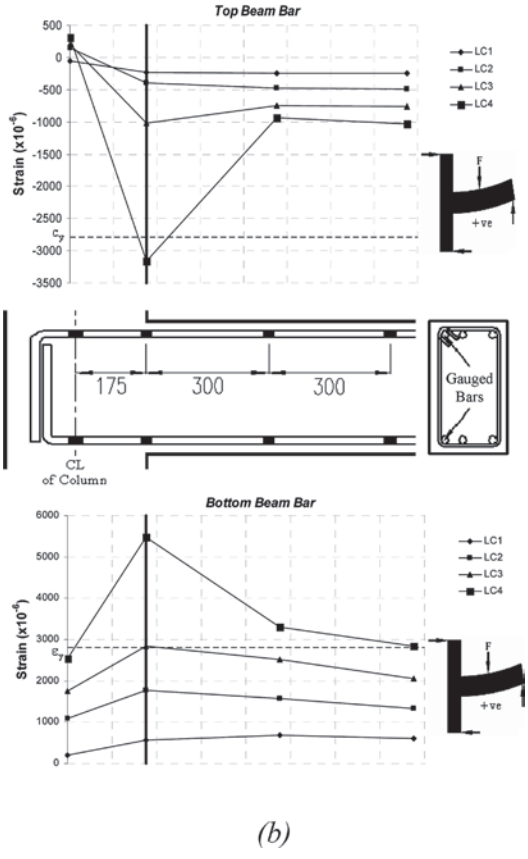

(b)

Fig. 10—Strain profiles of longitudinal beam bars of: (a) Specimen NS01; and (b) Specimen LS02. (Note: Dimensions in mm; 1 mm = 0.04 in.)

the joint region. Furthermore, the NS series specimens failed under extensive yielding of the beam longitudinal reinforcement accompanied with bond failure at the joint region. Therefore, the failures at the two different stages were suggested to be independent from each other.

For the LS series specimens, the differences between load at joint cracking and load at failure were higher, ranging from 46 to 60%. As suggested by the comparison between the NS series specimens, the amount of transverse reinforcements in the beams and columns had little effect on the overall strength of the test specimens. Therefore, the increase in strength for the LS series specimens could be primarily, if not solely, contributed to the strength of the transverse reinforcement in the joint region.

Longitudinal bar strains

The strain profiles from Specimens NS01 and LS02, as shown in Fig. 10, were selected to illustrate the differences in the distribution of strain between the two series, as it is not possible to present the results of all the specimens in this study. The peak strains in the beam and column bars at different stages of all specimens were summarized in Table 4. In the presentation, four load cases at four significant parts of the test were identified. They are the load conditions at which the first flexure crack is observed (LC1), load at which first joint crack occurred (LC2), load at which yielding of the test specimen (taken to be 75% of maximum load) occurred (LC3), and load at which the test specimen failed (LC4).

Strain profiles of Specimen NS01—The compressive strains in the top bars were generally small with a maximum strain of 800 μ at LC4. The distribution of compressive strains along the top bars at and away from the column face was relatively constant. Strains in the center of the joint core remained minimal throughout the test, showing no sign of strain penetration. In general, the small compressive strain in the top beam bars implied that most of the compressive forces were carried by the concrete. No crushing of concrete was observed throughout the tests.

In the bottom bars, between LC1 to LC3, strains along the bars increased gradually with an increase in load. Unlike the top bars, where strains at the center of the joint core remained small throughout, strains in the bottom bars increased gradually under increasing load. This was consistent with the observed bond-splitting crack seen from LC2 onward, which also showed signs of tensile strain penetration of the bottom beam longitudinal bars into the joint core.

Yielding of the bottom bars was observed just after LC3. At LC4, strains measured in the joint core were greater than that observed at the column face, indicating yield penetration into the joint core, which was consistent with the cracking patterns where severe bar pullout and wide diagonal shear cracks in the joint were observed. It could be expected that the bond forces diminished along the straight portion of the bottom beam bars from the inner column face to the hook and the steel tensile forces were resisted around the bend of the hook. At the end of LC4, yielding spread over a length of $1.5h_b$, where h_b is the beam depth.

Strain profile of Specimen LS02—In the top beam bars, a gradual and relatively consistent increase in compressive strain up to LC4 was observed at 475 and 775 mm (18.7 and 30.5 in.) from the column centerline. Strains were generally small at these locations with compressive strains reaching only 35% of the bar yield strains at LC4.

Table 4—Longitudinal bar strains, μ

	Joint cracking				Specimen failure			
	Beam bar		Column bar		Beam bar		Column bar	
Specimen	Tension	Compression	Tension	Compression	Tension	Compression	Tension	Compression
NS01	2474	–407	940	–208	4171	–781	1779	—
NS02	2013	–498	930	–201	2921	–571	2000	–357
NS03	1669	–326	524	–320	3401	–611	1327	–683
LS01	1298	–334	1211	–636	2913	–1695	3668	–1452
LS02	1770	–396	1488	–442	5469	–3160	4990	–1265
LS03	1609	–378	1317	–375	7895	–3086	4426	—

Most of the compressive forces were suggested to be carried by the concrete. Compressive strains measured at the interface of the column (175 mm [6.9 in.]) from the column centerline) were initially small but began to increase gradually after LC2. Between LC3 to LC4, a rapid increase in strain exceeding yield was observed. This coincided with the observed minor crushing of concrete cover at the inner face of the upper column, adjacent to the joint where the flexure compression zone was located.

Small tensile strains measured in the top beam bars located at the column centerline were in disagreement with flexural action. It was possible that the strain readings might have been affected by the intersecting column bars and/or the result of joint distortion.

In the bottom beam bars, tensile strains were measured over the entire gauged length of the bars. A gradual increase in tensile strain was observed up to LC3 at all locations. It was noted that at 175 mm (6.9 in.) from the column centerline, strain readings were slightly higher compared to the rest of the location, reaching yield strain at the end of LC3.

In loading to LC4, tensile yielding of the bottom beam bars was observed at all locations outside the joint region. The highest tensile strain of 5469 μ strains was measured at the beam-column interface, whereas strains further away from the joint region had reached yield. Yield penetration into the joint core was not observed, although it was expected that some yield penetration into the joint region had occurred between the center of the joint and the beam-column interface.

Comparison of strain profiles—With reference to Tables 3 and 4, it was observed that, although the load at joint cracking was higher in the LS series specimens, the observed tensile strains in the beam bars were relatively smaller but with higher tensile strains in the column bars. Similar observations were made for the bars under compression. At failure load, the measured strains in the specimens of the LS series were, in general, higher, which was expected, as the test specimens had attained higher loads. Furthermore, strains in the column bars of the NS series specimens remained relatively small, even at failure load. It was suggested that premature bar pullout failure occurred before sufficient load could be transferred into the columns.

The strain results provide valuable information on the effectiveness of force transfers between the elements that translate into the distribution of moments. The NS series specimens were not as effective in moment distributing because yielding and bond failure of the beam longitudinal bars occurred before forces were effectively transferred into the joint and to the column. The LS series specimens performed better because additional bottom beam longitudinal reinforcement, together with joint transverse reinforcement, was provided in the improved design. The contribution that each component provides needs to be investigated through a parametric study.

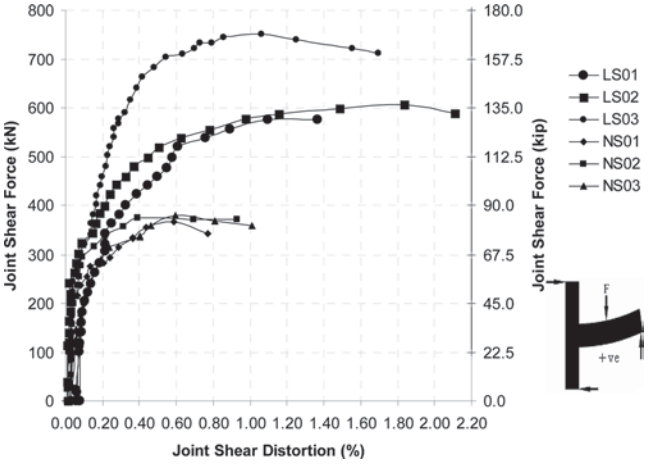

Fig. 11—Comparison of joint shear distortion.

Joint behavior

Joint shear—The combined plot of the joint shear force versus joint shear distortions of the test specimens are shown in Fig. 11. It can be noted that, as will be presented in the subsequent section, only the LS series specimens failed dominantly in joint shear. Joint shear capacity V_j is estimated based on Vollum[10] proposed a simplified design method given by

$$V_j = V_c + \left(A_{sje} f_y - \alpha b_e h_c \sqrt{f'_c}\right) \quad (1)$$

where V_c is the joint strength without joint transverse reinforcement given by

$$V_c = 0.642\beta\left(1 + 0.555\left(2 - h_b/h_c\right)\right) b_e h_c \sqrt{f'_c} \quad (2)$$

For the NS series specimens, the observed profiles were almost identical, with a slight deviation at the later stages of the test. This was expected, as their joint detailing and the strength of concrete were identical. At the joint shear force of approximately 370 kN ($0.55\sqrt{f'_c}$), the specimens failed as a result of extensive yielding and bond failure at bottom beam longitudinal reinforcements. Joint shear capacities for the NS series specimens were calculated to be 629.8 kN

($0.94\sqrt{f'_c}$). On average, joint shear distortions were small, measuring at 0.52%.

For the LS series specimens, two different profiles were observed. The profiles of Specimens LS01 and LS02 were similar, whereas a different profile was observed for Specimen LS03. This can be explained as both Specimens LS01 and LS02 have two sets of transverse links in the joint region (with different spacing), whereas Specimen LS03 had four sets. The additional transverse links increased the joint shear capacities of the specimen. Joint shear capacities of Specimens LS01 and LS02 were calculated to be 667.8 kN ($1.0\sqrt{f'_c}$), whereas Specimen LS03 was 758.8 kN ($1.13\sqrt{f'_c}$). In general, a steeper curve and a smaller joint distortion were observed for Specimen LS03. It was observed that for Specimens LS10 and LS02, joint shear distortion began to increase more rapidly as the joint shear force exceeds 540 kN ($0.8\sqrt{f'_c}$). For Specimen LS03, it was when the joint shear force exceeds 720 kN ($1.07\sqrt{f'_c}$). The joint shear capacities calculated based on the Vollum[10] proposed simplified design method proved to be a good conservative estimate.

The joints in the LS series specimens (with the exception of Specimen LS03) were said to have failed under excessive tensile stresses. The principle tensile stress for Specimens LS01 and LS02 at failure were calculated to be $0.86\sqrt{f'_c}$ and $0.90\sqrt{f'_c}$, respectively. Based on the failure criteria suggested by Priestley and Calvi,[11] the diagonal tension strength limit can be estimated to $0.29\sqrt{f'_c}$, which was exceeded by all the specimens. On the other hand, principle compression stresses for all the specimens were still within the diagonal compressive strength limit given by $0.25f'_c$ ($1.37\sqrt{f'_c}$ for f'_c = 30 MPa). Note that as there is no axial load on the specimens; the principal tensile stress is equal to the principle compression stress. For Specimen LS03, the principal compression stress was calculated to be $1.13\sqrt{f'_c}$ ($<1.37\sqrt{f'_c}$). Although the principal compression stress was smaller than the stipulated limit, the observed cracking patterns suggested that crushing of the concrete strut in the joint resulted in the failure of the specimen. This could explain and/or be supported by the steep negative gradient of the force-deflection curve after attaining maximum load, which was different for Specimens LS01 and LS02.

Therefore, although the increase in the amount of joint transverse reinforcement increased the joint shear strength of the specimens, a limit on its effectiveness exists. This is especially so if the mode of failure changed, as illustrated between the LS series specimens. This limit, however, required detailed parametric study, which is not within the scope of this study.

Bond stress—Bond stress is the stress developed by the force tending to produce movement or slippage at the interface between the concrete and the metal reinforcement bars. In the experiment, average bond stresses were obtained by dividing the difference of forces between two consecutive gauge points by the nominal surface area of the bar between them. Table 5 shows the maximum bond stresses developed in the longitudinal bars in the joint region during the test. Also shown are the corresponding load cases at which maximum bond stresses were developed. It can be noted that bond stresses with corresponding load at LC4 were not the absolute maximum values, but were the values attained at peak load.

For the NS series specimens, although the bond stresses in the bottom beam bars subjected to tension forces were relatively comparable, bond deterioration occurred at a much earlier stage (LC2) for Specimen NS01, compared to Specimens NS02 and NS03 (LC3). The increasing bond stresses developed under both tension and compression forces in the column bars were observed to increase with increasing amounts of transverse reinforcements in the elements. It was suggested that the increase in transverse reinforcement in the beams and columns adjacent to the joint region had some (but limited) confining effect that influenced the bond conditions in the joint region.

For bond stresses in the top beam bars that were subjected to compressive forces, bond stresses were observed to have decreased with the increase in transverse reinforcement. This, however, was because the recorded bond stresses had not attained maximum value, even at failure load (LC4). One should not mistake this as having contradicted the previous discussion. It was also suggested that the increase in transverse reinforcement in the beam provided better confinement to the concrete. Therefore, more compressive forces were transferred by the concrete into the joint core and less by the reinforcing bars. This resulted in smaller bond stresses being developed in the bars.

Similarly, for the LS series specimens, bond stresses in the beam bars subjected to tension forces were observed to be higher for specimens with higher transverse reinforcement ratios in the joint region. For bond stresses in the column bars subjected to tensile force, no significant difference in the maximum bond stresses were observed. It was observed, however, that maximum bond stresses were developed at earlier stages for specimens with higher transverse reinforcement ratios in the joint region (LC4, LC2, and LC1 for Specimens LS01, LS02, and LS03, respectively).

Table 5—Maximum bond stresses in joint, MPa

	Beam bar		Column bar	
Specimen	Tension	Compression	Tension	Compression
NS01	6.2 (LC2)	7.2 (LC4)*	1.3 (LC3)	3.2 (LC3)
NS02	6.1 (LC3)	5.8 (LC4)*	2.8 (LC3)	6.1 (LC4)*
NS03	5.6 (LC3)	3.2 (LC4)*	3.6 (LC4)*	8.6 (LC4)*
LS01	3.8 (LC3)	13.6 (LC4)*	5.2 (LC4)*	17.1 (LC4)*
LS02	7.4 (LC3)	17.8 (LC4)*	2.9 (LC2)	16.3 (LC4)*
LS03	10.1 (LC3)	17.1 (LC4)*	3.1 (LC1)	12.0 (LC4)*

*Bond stresses attained at failure load (not absolute maximum).
Note: 1 MPa = 145 psi.

The development of the strut-and-truss mechanism due to the addition of transverse reinforcement in the joint region seemed to have affected the internal flow of forces in the joint region, which ultimately influenced the bond condition of the column bars. For bond stresses in the column bars and beam bars in the joint region subjected to compressive forces, maximum bond stresses were not attained at the failure load (LC4).

Between specimens of the different series, it was observed that maximum bond stresses in the beam and column bars were generally higher in the LS series specimens. Furthermore, it can be noted that higher bond stresses were observed in reinforcing bars subjected to compressive forces, where the effect of concrete confinement was greater.

Decomposition of deflection

Table 6 shows the summary of the decomposition of deflection of the test specimens. Due to space limitation, only two particular load cases (LC2 and LC4) are presented. In general, it was observed that the total accounted deflections ranged from 60 to 90%. Higher percentages of the unaccounted deflections were usually observed at early stages because during the initial stages of the loading process, the total deflections measured might be overestimated due to the rigid body movement of the subassemblages, taking into consideration the allowances in the test setup. Furthermore, it can be noted that not all locations were gauged due to the arrangement and limitation of the test setup. Therefore, locations where significant deformation occurred might not have been measured. Fluctuating results were affected by small readings, especially in the areas of shear deformation.

In general, the main mechanism resisting the increase in load is represented by the component with the highest percentage. Therefore, the modes of failure of the specimens can be implied from the contribution distributions.

When comparing the contribution from different components, it was observed that for the NS series specimens, the dominant mechanism in resisting the increase in load at early stages was from the beam flexural action. The percentage of contribution from this component ranges from 17 to 28%. At failure stage, however, beam fixed-end components became the dominant mechanism, with the percentage of contribution ranging from 19 to 23%.

Similarly, for the LS series specimens at early stages, the contribution due to the beam flexure component was the dominant resisting mechanism with the percentage of contribution ranging from 26 to 34%. Unlike the NS series specimens, joint shear became the major contributing component at the failure stage.

Based on this observation, and from the cracking patterns discussed previously, the failures of the NS series specimens consist of joint shear failure at the initial stage, and bar pullout failure resulted from bond slip in the beam longitudinal bars. For the LS series specimens, the distress of the joint, which included severe shear distortion and cracking of the concrete cover, resulted in the failure of the specimens.

CONCLUSIONS AND DISCUSSIONS

Based on the test results described in this study, the following conclusions can be drawn.

1. In the experimental study, test specimens were loaded monotonically beyond their service loading until failure was observed. The test results obtained were satisfactory in terms of strength under monotonic loading, simulating gravity load from the floor service loading. The performance of the specimen in the improved design (Specimen LS03) was found to be superior to that of Specimens LS01 and LS02 from the same series, which in turn were superior to the specimens in the as-built design. Better performance was suggested to have resulted from the provision of transverse reinforcement in the joint region and the additional longitudinal beam bars, as evidenced from the test results.

2. The increase in the percentage of transverse reinforcement in the joint region improved the shear strength of the joint through the development of the truss mechanism. The test results from the specimens of the improved design (LS series), however, showed that joint shear failure was still the dominant failure mode and is independent of the amount of joint transverse reinforcement. Furthermore, it was important to note that undesired brittle failure mode (crushing of concrete struts) can result due to the insufficient compression area with respect to the forces acted on the joint, as evidenced in Specimen LS03.

3. Premature bond failure was observed in the bottom beam bars in all NS series specimens. It was suggested that the presence of joint transverse reinforcement could prevent or limit bond failure of the beam longitudinal bars.

4. Test results on the increase in provision of transverse reinforcement in the beam and column elements adjacent to the joint panel showed no significant influences on the strength of the exterior beam-column subassemblages. The total deformations, however, were significantly reduced.

In the study of progressive collapse, it is important to understand that every element/joint is critical for load transfer and moment redistribution. Failure in any of the elements/joints will result in the increase in load and moment of adjacent members, which often result in collapse.

Table 6—Decomposition of deflection, %

	NS01		NS02		NS03		LS01		LS02		LS03	
Load stage	LC2	LC4	LC2	LC4	LC2	LC4	LC2	LC4	LC2	LC4	LC2	LC4
Unaccounted	33	28	39	23	49	31	37	26	36	10	20	27
Joint shear	8	16	5	13	5	13	12	21	6	28	8	17
Column shear	1	7	3	3	4	4	4	6	0	8	6	8
Column flexure	6	8	8	13	8	13	8	12	9	15	13	14
Beam shear	6	4	4	4	3	3	2	3	5	4	6	5
Beam flexure	28	18	27	21	17	13	26	16	34	15	34	15
Beam fixed-end	18	19	14	23	14	23	11	16	10	20	13	14

In the context of the exterior beam-column subassemblage in this investigation, with the onset of bar pullout failure, as observed in the NS series specimens, a significant amount of moment will be redistributed to the adjacent member/frame, as illustrated in Fig. 1. If the adjacent members are not able to carry the increase in load and/or moment, it will fail and possibly cause collapse. On the other hand, specimens of the improved design performed better and were able to redistribute a significant amount of moment within itself (between the beam and columns).

ACKNOWLEDGMENTS

This research was supported by a research grant provided by the Defense Science and Technology Agency (DSTA), Singapore, under the Protective Technology Research Center, Nanyang Technological University, Singapore. Any opinions, findings, and conclusions expressed in this paper are those of the authors and do not necessarily reflect the view of DSTA, Singapore.

NOTATION

A_{sje} = cross-sectional area of joint transverse reinforcement placed within upper five-eighths of beam depth below tensile reinforcement in beam
b_e = effective joint width
C_b = compressive force in beam, kN (kip)
C_c = compressive force in column, kN (kip)
F = tie force induced by joint transverse reinforcement, kN (kip)
f'_c = concrete cylinder strength, MPa (psi)
f_u = ultimate strength of steel reinforcement, MPa (psi)
f_y = yield strength of steel reinforcement, MPa (psi)
h_b = effective depth of beam
h_c = depth of column
T_b = tension force in column, kN (kip)
T_c = tension force in beam, kN (kip)
V = shear force in column, kN (kip)
α = coefficient, which depends on factors including column load, concrete strength, stirrup index, and joint aspect ratio, can be conservatively taken as 0.2 and 2.4 (with f'_c in MPa and psi, respectively)
β = 1.0 and 0.9 for connections with L bars and U bars, respectively
ε_y = yield strain of steel

REFERENCES

1. ASCE 7-02 Standard, "Minimum Design Loads for Buildings and Other Structures," SEI, American Society of Civil Engineers, Washington, DC, 2002, 352 pp.

2. Griffiths, H.; Pugsley, A. G.; and Saunders, O., "Report of the Inquiry into the Collapse of Flats at Ronan Point, Canning Town," Her Majesty's Stationery Office, London, UK, 1968.

3. Hayes Jr., J. R. et al., "Can Strengthening for Earthquake Improve Blast and Progressive Collapse Resistance?" *Journal of Structural Engineering*, ASCE, V. 131, No. 8, Aug. 2005, pp. 1157-1177.

4. FEMA 403, "World Trade Center Building Performance Study: Data Collection, Preliminary Observations and Recommendations," 2002.

5. General Services Administration, "Progressive Collapse Analysis and Design Guidelines for New Federal Office Buildings and Major Modernization Projects, GSA," 2003.

6. U. S. Department of Defense, "Design of Buildings to Resist Progressive Collapse," Unified Facilities Criteria, UFC 4-023-03, Washington, DC, 2005.

7. Yi, W.-J.; He, Q.-F.; Xiao, Y.; and Kunnath, S. K., "Experimental Study on Progressive Collapse-Resistant Behavior of Reinforced Concrete Frame Structures," *ACI Structural Journal*, V. 105, No. 4, July-Aug. 2008, pp. 433-439.

8. CP 65, "Structural Use of Concrete, Part 1: Code of Practice for Design and Construction," Singapore Standard, Singapore, 1999.

9. BS 8110-1:1997, "Structural Use of Concrete, Part 1. Code of Practice for Design and Construction," British Standards Institution, 1997, 168 pp.

10. Vollum, R. L., "Design and Analysis of Beam-Column Joints," PhD thesis, University of London, London, UK, 1998.

11. Priestley, M. J. N., and Calvi, G. M., "Toward a Capacity-Design Assessment Procedure for Reinforced Concrete Frames," *Earthquake Spectra*, V. 7, No. 3, pp. 413-437.